# A new phase diagram for layered antiferromagnetic films

OLAV HELLWIG[1], TARYL L. KIRK[1,2], JEFFREY B. KORTRIGHT[3], ANDREAS BERGER[1] AND ERIC E. FULLERTON*[1]

[1]IBM Almaden Research Center, San Jose, California 95120, USA
[2]Department of Physics, University of California-San Diego, La Jolla, California 92093, USA
[3]Materials Science Division, Lawrence Berkeley National Laboratory, Berkeley, California 94720, USA
*e-mail: eef@us.ibm.com

Published online: 12 January 2003; doi:10.1038/nmat806

Magnetic multilayer films provide convenient model systems for studying the physics of antiferromagnetic films and surfaces. Here we report on the magnetic reversal and domain structure in antiferromagnetically coupled Co/Pt multilayers that are isomorphic to layered antiferromagnetic films with perpendicular magnetic anisotropy. We observe two distinct remanent states and reversal modes of the system. In mode 1 the magnetization in each layer reverses independently, producing an antiferromagnetic remanent state that shows full lateral correlation and vertical anticorrelation across the interlayers. In mode 2 the reversal in adjacent layers is locally synchronized with a remanent state that is vertically correlated but laterally anticorrelated in ferromagnetic stripe domains. Theoretical energy calculations of the two ground states identify a new phase boundary that is in good agreement with our experimental results.

The response of antiferromagnetic (AF) materials in an applied field has interested researchers since predictions by Néel of a spin-flop phase transition in AF crystals with uniaxial anisotropy[1]. The topic has attracted renewed interest because AF films have become a key building block and integral part of modern magnetic technologies, such as magnetic recording heads[2]. As such, considerable effort is applied to understanding the magnetic structure in AF films and the interaction with adjacent ferromagnetic films[3]. New techniques for imaging AF domains in thin films have been recently reported[4], but the field dependence and hysteresis behaviour of AF materials in the thin-film geometry remain open questions.

The atomic-level control currently available in thin-film deposition[5] now allows one to engineer AF-coupled ferromagnetic films into artificial AF film structures that provide new insights into the field dependence of AF films and surfaces[6–10]. Such structures are particularly attractive for studying field-induced phase transitions in AF films because the exchange interaction that couples adjacent ferromagnetic layers is comparable to the Zeeman energy in modest applied fields. In addition, finite size and surface effects are more pronounced than in AF crystals. For example, the surface spin-flop transition (the corresponding surface phase transition to the original bulk transition identified by Néel) was predicted by Mills to occur at the surfaces of AF crystals[11]. However, this transition has only been observed experimentally in magnetic multilayers with uniaxial in-plane anisotropy[9]. These experiments have, in turn, motivated renewed interest in the theoretical understanding of finite and semi-infinite AF systems (see for example ref. 12).

Here we describe the domain formation and reversal in AF-coupled multilayers with perpendicular magnetic anisotropy. The system is based on the well-studied Co/Pt multilayers with perpendicular magnetic anisotropy[13], which are periodically interleaved with Ru layers to introduce AF interactions to the system[14]. The resulting $[[Co/Pt]_{X-1}/Co/Ru]_N$ multilayers are made up of $N$ ferromagnetic $[Co/Pt]_{X-1}/Co$ sublayer stacks with perpendicular anisotropy with each AF-coupled to the adjacent sublayers. A similar structure has been discussed previously[15].

In ferromagnetic thin films with perpendicular anisotropy the balance between exchange, anisotropy and dipolar energies often results in stripe domain patterns as first described by Kittel[16]. The characteristic width of the periodic or quasi-periodic domains varies with film thickness $t$, and the domain morphology depends sensitively on the field history. Domains can be arranged in a variety of metastable configurations (for example, aligned or labyrinth stripe domains, and bubble domains) and hysteresis effects are connected with their generation, annihilation and transformation with applied field[16–22]. The AF coupling controllably alters the typical energy balance between the dipolar and domain wall energies in perpendicular thin films producing competing reversal modes for the composite system. These modes produce distinct remanent states that are either laterally correlated in an antiferromagnetic configuration or vertically correlated forming ferromagnetic stripe domains. We describe the experimental observation of these two modes and the transition from one mode to the other with increasing film thickness, and we compare the results of model calculations to the experimentally determined phase diagram.

The multilayer structures used were $[[\mathrm{Co}(4\ \text{Å})/\mathrm{Pt}(7\ \text{Å})]_{X-1}/\mathrm{Co}(4\ \text{Å})/\mathrm{Ru}(9\ \text{Å})]_N$ where $2 \le X \le 10$ and $2 \le N \le 12$. The samples were deposited by magnetron sputtering (3 mT Ar pressure) onto ambient-temperature Si substrates coated with $Si_3N_x$ and onto $Si_3N_x$ membranes coated with 200-Å Pt seed layers. A series of $[\mathrm{Co}(4\ \text{Å})/\mathrm{Pt}(7\ \text{Å})]_X$ multilayers was also grown to characterize the magnetic properties of individual sublayer stacks. X-ray diffraction measurements confirm the multilayer structure has a (111) crystalline texture. The average magnetic properties were determined by superconducting quantum interference device (SQUID) and magneto-optical Kerr effect (MOKE) magnetometry, and the domain structure was characterized by magnetic force microscopy (MFM) and resonant soft X-ray small-angle scattering (SAS) in a transmission geometry[23]. The SAS experiments were done at the Advanced Light Source (located at the Lawrence Berkeley National Laboratory, California, USA) on undulator beamlines 4.0 and 8.0 with the photon energy tuned to the Co $L_3$ resonant peak (778 eV) to maximize the magnetic scattering contrast.

Magnetic hysteresis loops with the field perpendicular to the films are shown for the samples with $N = 4$ and $X = 8$ and 10 in Fig. 1 together with the corresponding field-dependent SAS intensities. For $X = 8$ there are discrete steps in the hysteresis loop, with stable magnetization plateaux at $M/M_s$ values of 0.5, 0 and –0.5, where $M$ is magnetization and $M_s$ is saturation magnetization. We refer to this step-like reversal as mode 1 with each of the four AF-coupled Co/Pt sublayer stacks reversing independently at different external fields. Using the depth sensitivity of MOKE we determined the switching sequence of the four Co/Pt sublayers as the 3rd, 1st, 4th, 2nd in going from positive to negative saturation, similar behaviour to that described previously[15]. The remanent state is illustrated in the upper inset of Fig. 1a. The switching behaviour is confirmed by the field-dependent SAS intensity measurements in Fig. 1b. Because magnetic SAS is due to lateral deviations from uniform magnetization, the observed scattering arises from domain formation during reversal of the layers[23]. The separate switching of the four Co/Pt stacks is clearly visible as four distinct scattering peaks indicating that each layer reverses by domain nucleation and propagation that is independent of the adjacent layers. The scattering intensity drops back to the baseline value after each of the four switching processes where the intermediate stages of reversal (the plateaux in the hysteresis loop) possess few or no domains.

Moderately increasing the Co/Pt repetitions within each stack from $X = 8$ to 10 has a marked effect on the hysteresis behaviour. Instead of layer-by-layer switching, we observe a hysteresis loop that is characterized by cooperative reversal of all the layers. The corresponding SAS intensity profile in Fig. 1b (open symbols) confirms the significant change in the reversal behaviour. The broad, 50-fold scattering intensity increase shows that domains are present throughout the entire reversal process. Both the hysteresis loop and SAS intensity

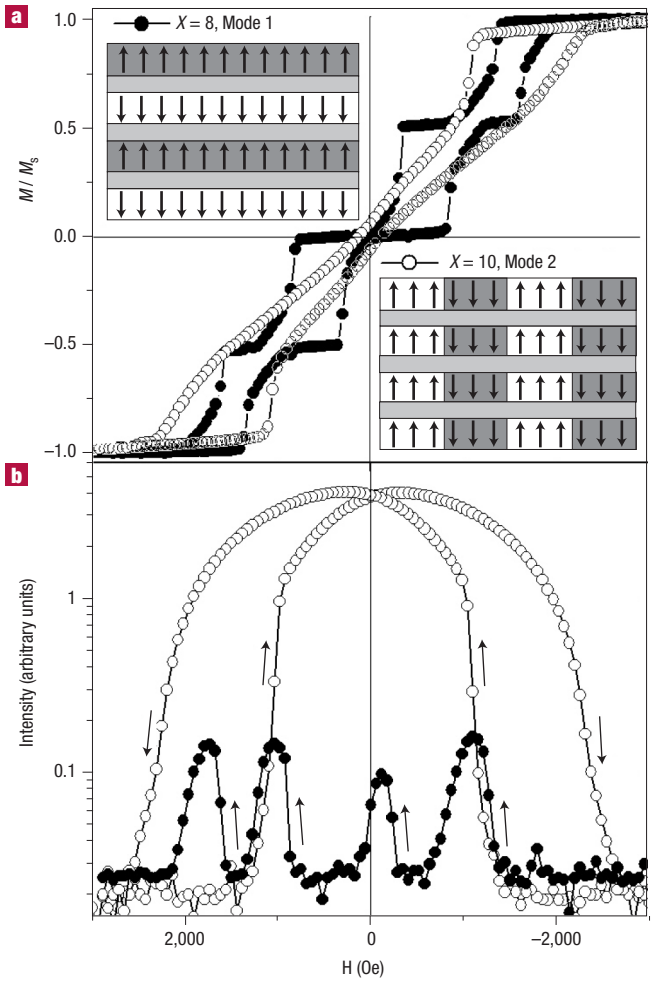


**Figure 1 Magnetic hysteresis and small-angle scattering (SAS) results for AF-coupled multilayers with different magnetic layer thicknesses. a**, Out-of-plane magnetization and **b**, soft X-ray SAS intensity against applied field $H$ for $N = 4$ and $X = 8$ and 10 multilayers of $[(\mathrm{Co/Pt})_{X-1}/\mathrm{Co/Ru}]_N$. $M$ is magnetization, $M_s$ is the saturation magnetization. The SAS intensity was measured with in-plane wavevector $q = 0.0035\ \text{Å}^{-1}$. The arrows in **b** indicate the field-sweep direction. For clarity only the descending branch is shown (solid symbols) for the $X = 8$ sample in **b**. The marked change in both the loop shape and scattering intensity indicate a change in the reversal mode. The insets in **a** illustrate the remanent magnetic configurations proposed for the two samples where the arrows indicate the magnetic configuration of each Co/Pt sublayer separated by a Ru layer.

profile are similar to that observed for Co/Pt multilayers with the same total thickness—that is, a purely ferromagnetic film[22]. In contrast to the $X = 8$ sample, this sample reverses by means of ferromagnetic domains that are vertically correlated through the film and evolve continuously with field. We refer to this continuous reversal as mode 2 and its remanent state is shown schematically by the lower inset of Fig. 1a. Supplementary SAS scans in the remanent state indicate that the average domain size is also similar to that observed for Co/Pt multilayers with the same total thickness.

To further characterize the transition between the two modes, we compared the initial magnetization loops after in-plane saturation with the major loops, as well as MFM measurements in the remanant domain state after in- and out-of-plane saturation. The results are shown in Fig. 2 for a sequence of samples with $N = 4$ and $X = 7$–10. In the left column

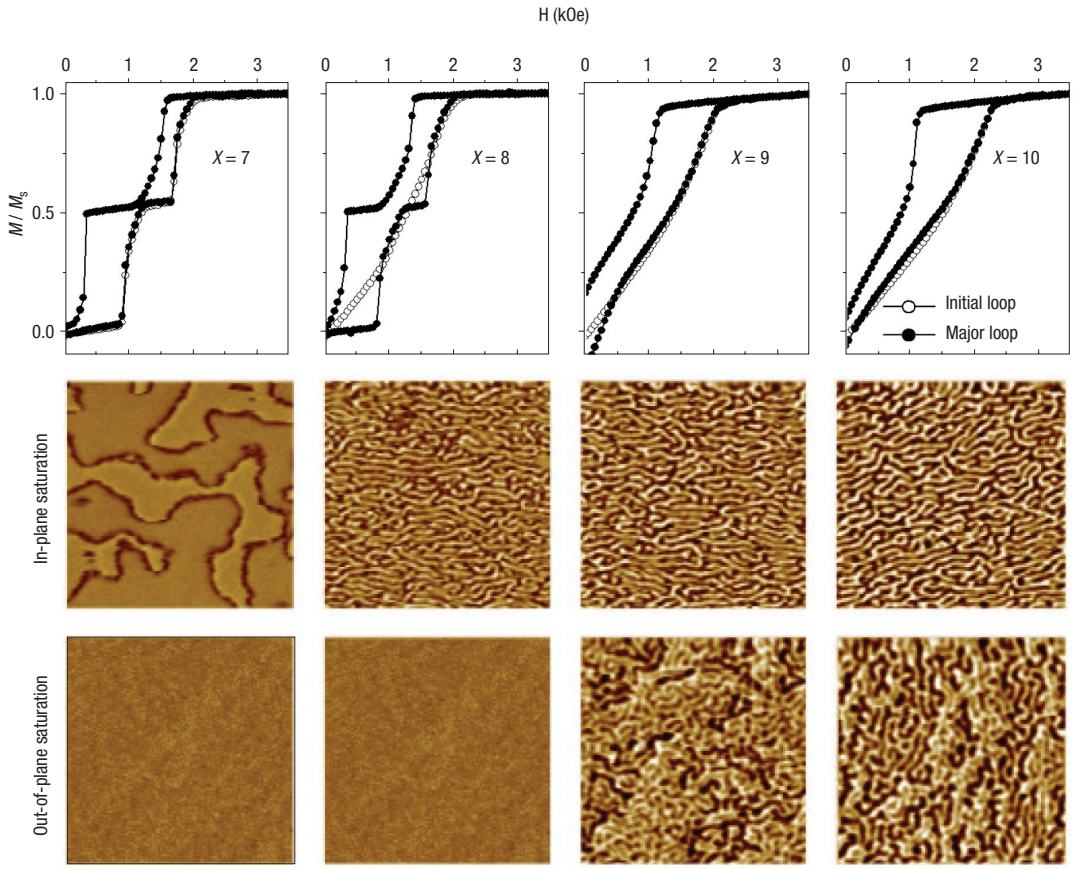


**Figure 2 Out-of-plane SQUID measurements and MFM images of $[(Co/Pt)_{X-1}/Co/Ru]_N$ multilayers with $N = 4$ and $X = 7–10$.** The magnetization data in the top row show the initial loops after in-plane saturation (open symbols) as well as the upper quadrant of the major loop (solid symbols). The second row displays MFM images of the remanent domain structure as obtained after in-plane saturation. The bottom row shows corresponding MFM images after out-of-plane saturation. Each MFM image is $5 \times 5\ \mu m^2$ in size.

($X = 7$) we observe mode 1 behaviour in the major loop as well as after in-plane saturation. That is, the initial loop falls on top of the major loop. MFM reveals large-scale domains after in-plane saturation. The domains consist of either up–down–up–down or down–up–down–up magnetization configurations. Antiphase boundaries between these two antiferromagnetic configurations produce the visible contrast in the image. Going back to remanence after out-of-plane saturation populates one AF configuration and no domain structure is observed within the image area.

In the second column ($X = 8$) we add one more Co/Pt repetition to each of the AF-coupled stacks, and the sample reveals characteristics of both modes. Whereas the major loop is stepped with a mode 1 reversal (Fig. 1), the initial loop after in-plane saturation shows continuous switching typical of mode 2. MFM images confirm the dualistic behaviour of this sample. In-plane saturation creates a stripe domain structure similar to those observed without any Ru layers, showing strong contrast consistent with up and down domains that penetrate through the entire film[23]. Out-of-plane saturation puts the system into the AF-coupled, domain-free state. Adding more Co/Pt repetitions (columns 3 and 4 of Fig. 2) results in a complete transition into mode 2. The initial and major loops both become continuous and MFM images show perpendicular up and down stripe domains independent of the field history.

Up to now we have considered only multilayers with $N = 4$ sublayer stacks. To obtain a more general picture of the transition between modes 1 and 2, we examined samples with different $X$ and $N$ values. Each sample was characterized by magnetometry and MFM and the reversal behaviour classified as mode 1, or mode 2, or mixed where the major loop showed mode 1 reversal whereas the initial loop after in-plane saturation showed mode 2 reversal. Figure 3a summarizes the results in a phase diagram by plotting $N$ against $X$ and coding the three different reversal categories. We find that the reversal mode depends on both $X$ and $N$ where large $X$ and $N$ tend towards mode 2 behaviour.

To understand these systematics we compare the energy contributions to modes 1 and 2 in the remanent states as shown schematically in Fig. 1. For mode 1, the magnetic energy per unit area $E_1$ is determined by the magnetostatic and interlayer exchange energies and is given by

$$E_1 = N2\pi M_s^2 t - (N-1)J_{ex} \qquad (1)$$

where $t$ is the sublayer thickness and $J_{ex}$ is the interlayer coupling strength across the Ru layer. For a film uniformly magnetized perpendicular to the layer, the magnetostatic energy is $2\pi M_s^2 t$, and because no dipolar fields exist outside a uniformly magnetized film, the $N$ uniform layers add independently of the magnetization directions. The interlayer coupling energy depends on the number of Ru layers and on $J_{ex}$. For mode 2, the energy $E_2$ will depend on the magnetostatic energy $E_{mag}$, the domain wall energy $E_{wall}$ and interlayer exchange energies:

$$E_2 = E_{mag} + E_{wall} + (N-1)J_{ex} \qquad (2)$$

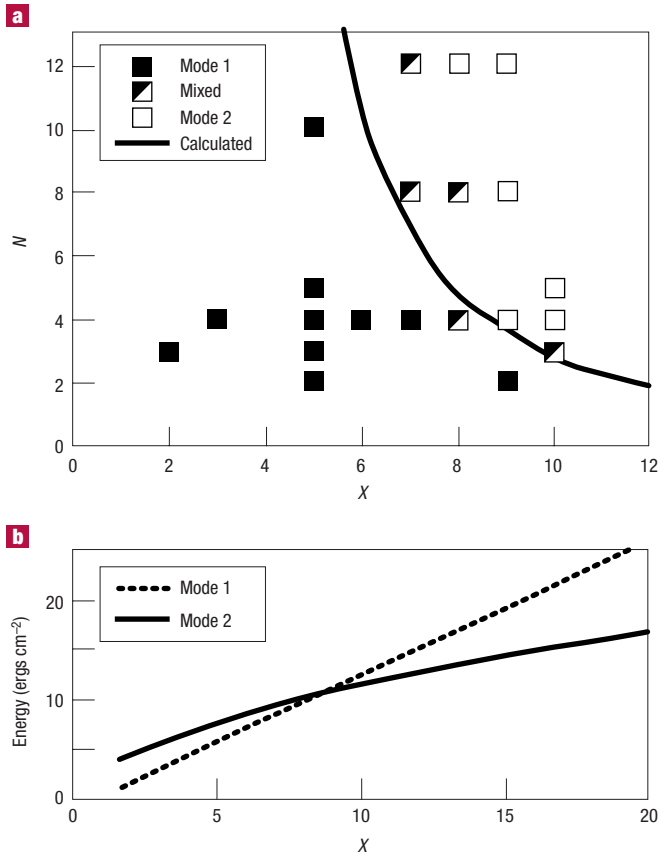


**Figure 3** **a**, Phase diagram of the magnetic reversal modes in $[(Co/Pt)_{X-1}/Co/Ru]_N$ multilayers depending on *N* and *X*. Samples that show a mode 1 reversal after out-of-plane saturation and a mode 2 reversal after in-plane saturation are considered mixed mode. The solid line is the calculated phase boundary described in the text. **b**, Calculated magnetic energy of the mode 1 and mode 2 remanent configurations against *X* for $N = 4$.

where the interlayer exchange energy enters with the opposite sign because adjacent layers are parallel. The magnetostatic energies need to be calculated for the particular domain structure. For simplicity we consider the magnetostatic energy of a uniform film of thickness $Nt$ with stripe domains of width $D$. This energy $E_{mag}$ can be estimated as described previously[24]:

$$E_{mag} \approx \frac{16M_S^2 D}{\pi^2}\sum_n^{odd}\frac{1}{n^3}[1-\exp(-n\pi Nt/D)] \qquad (3)$$

This assumes the domain wall width is small compared with $D$ and that the spins remain perpendicular to the film. This equation can be generalized to consider the effects of relaxation of the spins away from the surface normal[16–18], formation of closure domains[18,25,26], and the multilayer structure[26]. However, equation (3) is sufficient to understand the current results. The domain wall energy is given by

$$E_{wall} \approx \frac{4\sqrt{(AK_U)}Nt}{D} \qquad (4)$$

where $A$ is the atomic exchange ($\sim 10^{-6}$ erg cm) and $K_U$ is the uniaxial perpendicular anisotropy constant[18].

Shown in Fig. 3b is a comparison of modes 1 and 2 (equations (1) and (2), respectively) for $N = 4$ and the experimentally determined parameters for our samples ($M_s = 700$ e.m.u. cm$^3$, $K_U = 5 \times 10^6$ erg cm$^{-3}$, $J_{ex} = 0.45$ erg cm$^{-2}$ and $t = X\Lambda$ where $\Lambda = 11$ Å is the Co/Pt bilayer period). For each value of $X$, we first minimize the energy expression in equation (3) with respect to the domain size $D$ for that total film thickness. After determining $D$, we then calculate the total energy of the domain structure according to equations (2) and (3). The AF state (mode 1) is energetically favourable at low $X$, whereas the domain state (mode 2) is favourable at high $X$ with a transition between $X = 8$ and 9 as observed experimentally. Further calculations for varying $N$ allow us to draw a theoretical boundary into the phase diagram (solid line, Fig. 3a) that separates mode 1 from mode 2 samples. If $J_{ex}$ is set to zero, then equations (1) and (2) describe the energy of a uniformly magnetized film relative to the stripe domain state where the domain state is always energetically favoured over the uniform state. For $J_{ex} > 0$ (that is, for AF coupling), however, there is an additional energy $2(N-1)J_{ex}$ that favours the laterally correlated AF configuration. Only when the magnetostatic energy gains of the domain state overcome this threshold energy do vertically correlated domains become favoured. Once formed, the domain size is independent of $J_{ex}$ and only depends on the balance between magnetostatic and domain wall energies as it does in a single ferromagnetic film with perpendicular anisotropy.

These calculations are based on the free energy of the remanent state. That is, they represent properties of the thermal equilibrium that may, but does not have to, be fulfilled during a hysteretic magnetization reversal process. The close agreement between our remanent model and the experimental observations, however, suggests that the non-equilibrium process of domain nucleation at the onset of the reversal is driven by the same type of energetics. As for the equilibrium state, there are essentially two ways for a nucleation domain to form. It can be dominated by the interlayer exchange coupling, which drives lateral growth of a nucleated domain in a layer, and leads to the separated reversal of individual layers. If, on the other hand, the dipolar energy dominates the nucleation process, the switching of individual sublayers will be locally synchronized during nucleation, and these vertically correlated domains evolve into the stripe domain state observed at remanence. The domain nucleation as the crucial magnetization reversal step is driven by similar energy terms (with slightly altered geometric factors in $E_{mag}$) as the equilibrium ground state, and explains the fundamental change of the magnetization reversal mode observed in a small parameter window. The mixed-mode behaviour near the transition region suggests that mode 1 reversal behaviour is slightly favoured in the hysteretic out-of-plane magnetization reversal process. It should be noted that the present results and calculations apply to films where the perpendicular anisotropy ($K_U$) is larger than the shape anisotropy ($K_U > 2\pi M_s^2$) and $K_U t$ is greater than the interlayer coupling ($J_{ex}$). If these conditions are not met, then additional magnetic configurations such as closure magnetic domains[26] or reversal by surface and bulk spin-flop transitions become possible[9].

Here we have discussed the transition between the two competing reversal modes with increasing film thickness, but we have also observed a similar transition by changing the measurement temperature and interlayer exchange strength. These results demonstrate that a variety of parameters can be tuned in such a way that the mode 1 and 2 remanent states are nearly equal in energy, allowing one to study this transition regime where novel domain structures, more complex reversal modes and interesting dynamic properties should be present.

Received 25 October 2002; accepted 28 November 2002; published 12 January 2003.

## References

1. Néel, L. Propriétés magnétiques de l'état métallique et énergie d'interaction entre atomes magnétiques. *Ann. Phys. (Paris)* **5,** 232–279 (1936).
2. Kools, J. C. S. Exchange-biased spin-valves for magnetic storage. *IEEE Trans. Magn.* **32,** 3165–3184 (1996).
3. Nogués, J. & Schuller, I. K. Exchange bias. *J. Magn. Magn. Mater.* **192,** 203–232 (1999).
4. Nolting, F. *et al.* Direct observation of the alignment of ferromagnetic spins by antiferromagnetic spins. *Nature* **405,** 767–769 (2000).
5. Kortright, J. B. *et al.* Research frontiers in magnetic materials at soft X-ray synchrotron radiation facilities. *J. Magn. Magn. Mater.* **207,** 7–44 (1999).
6. Camley, R. E. & Tilley, D. R. Phase transitions in magnetic superlattices. *Phys. Rev. B* **37,** 3413–3421 (1988).

7. Dieny, B. J., Gavigan, P. & Rebouillat, J. P. Magnetisation processes, hysteresis and finite-size effects in model multilayer systems of cubic or unitaxial anisotropy with antiferromagnetic coupling between adjacent layers. *J. Phys. Condens. Matter* **2,** 159–185 (1990).
8. Hood, R. Q. & Falicov, L. M. Itinerant-electron, one-dimensional magnetic superlattices. *Phys. Rev. B* **44,** 9989–9996 (1991).
9. Wang, R. W., Mills, D. L., Fullerton, E. E., Mattson, J. E. & Bader, S. D. Surface spin-flop transition in Fe/Cr(211) superlattices: Experiment and theory. *Phys. Rev. Lett.* **72,** 920–923 (1994).
10. Jiang, J. S. *et al.* Exchange-bias effect in Fe/Cr(211) double superlattice structures. *Phys. Rev. B* **61,** 9653–9656 (2000).
11. Mills, D. L. Surface spin-flop state in a simple antiferromagnet. *Phys. Rev. Lett.* **20,** 18–21 (1968).
12. Micheletti, C., Griffiths, R. B. & Yeomans, J. M. Surface spin-flop and discommensuration transitions in antiferromagnets. *Phys. Rev. B* **59,** 6239–6249 (1999).
13. Johnson, M. T., Bloemen, P. J. H., den Broeder, F. J. A. & de Vries, J. J. Magnetic anisotropy in metallic multilayers. *Rep. Prog. Phys.* **59,** 1409–1458 (1996).
14. Parkin, S. S. P., More, N. & Roche, K. P. Oscillations in exchange coupling and magnetoresistance in metallic superlattice structures: Co/Ru, Co/Cr, and Fe/Cr. *Phys. Rev. Lett.* **64,** 2304–2307 (1990).
15. Willekens, M. M. H. *et al.* in *Magnetic Ultrathin Films: Multilayers and Surfaces, Interfaces and Characterization, MRS Symp. Proc. 313* (eds Jonker, B. T. *et al.*) 129–135 (Materials Research Society, Pittsburgh, 1993).
16. Kittel, C. Theory of the structure of ferromagnetic domains in films and small particles. *Phys. Rev.* **70,** 965–971 (1946); Physical theory of ferromagnetic domains. *Rev. Mod. Phys.* **21,** 541–583 (1949).
17. Kooy, C. & Enz, U. Experimental and theoretical study of the domain configuration in thin layers of $BaFe_{12}O_{19}$. *Philips Res. Rep.* **15,** 7–29 (1960).
18. Hubert, A. & Schäfer, R. *Magnetic Domains* Ch. 3, 5 (Springer, Berlin, 1998).
19. Bochi, G. *et al.* Magnetic domain structure in ultrathin films. *Phys. Rev. Lett.* **75,** 1839–1842 (1995).
20. Gehanno, V., Samson, Y., Marty, A., Gilles, B. & Chamberod, A. Magnetic susceptibility and magnetic domain configuration as a function of the layer thickness in epitaxial FePd(001) thin films ordered in the L1(0) structure. *J. Magn. Magn. Mater.* **172,** 26–40 (1997).
21. Seul, M. & Wolfe, R. Evolution of disorder in two-dimensional stripe patterns: "Smectic" instabilities and disclination unbinding. *Phys. Rev. Lett.* **68,** 2460–2463 (1992).
22. Bobcock, K. L. & Wetervelt, R. M. Avalanches and self-organization in cellular magnetic-domain patterns. *Phys. Rev. Lett.* **64,** 2168–2171 (1990).
23. Kortright, J. B. *et al.* Soft x-ray small-angle scattering as a sensitive probe of magnetic and charge heterogeneity. *Phys. Rev. B* **64,** 092401 (2001).
24. Málek, Z. & Kamberský, V. Theory of the domain structure of thin films of magnetically uni-axial materials. *Czech J. Phys.* **8,** 416–422 (1958).
25. Hameed, S. *et al.* Analysis of disordered stripe magnetic domains in strained epitaxial Ni(001) films. *Phys. Rev. B* **64,** 184406 (2001).
26. Labrune, M. & Belliard, L. Stripe domains in multilayers: Micromagnetic simulations. *Phys. Status Solidi A* **174,** 483–497 (1999).


## Acknowledgements

Work at LBNL was supported by the Office of Science, Office of Basic Energy Sciences, Division of Materials Science of the US Department of Energy under contract DE-AC03-76SF00098. O.H. was partially supported by the Deutsche Forschungsgemeinschaft through a Forschungsstipendium under the contract number HE 3286/1-2.
Correspondence and requests for materials should be addressed to E.E.F.

## Competing financial interests

The authors declare that they have no competing financial interests.